# Aspect ratio and polydispersity dependence of isotropic-nematic transition in discotic suspensions

Andres F. Mejia,[1,4] Ya-Wen Chang,[1] Ratna Ng,[1] Min Shuai,[2] M. Sam Mannan,[1,4] and Zhengdong Cheng[1,2,3,4,*]

[1]*Artie McFerrin Department of Chemical Engineering, Texas A&M University, College Station, Texas 77843-3122, USA*

[2]*Materials Science and Engineering Program, Texas A&M University, College Station, Texas 77843-3003, USA*

[3]*Professional Program in Biotechnology, Texas A&M University, College Station, Texas 77843-3122, USA*

[4]*Artie McFerrin Department of Chemical Engineering, Mary Kay O'Connor Process Safety Center, Texas A&M University, College Station, Texas 77843-3122, USA*

(Received 22 March 2012; revised manuscript received 30 April 2012; published 20 June 2012)

We demonstrate the strong dependency of the isotropic-nematic (I-N) transition of discotic suspensions on the aspect ratio ($\xi$ = thickness/diameter) via control of the sizes of pristine ZrP crystals and subsequent exfoliation to monolayers. The size fractionation of the I-N transition facilitates the analysis of the effect of polydispersity. A systematic variation in the aspect ratio in the low aspect ratio region ($0.001 < \xi < 0.01$) showed that the I-N transition volume fraction increases with the aspect ratio in agreement with computer simulations. It was found that the transition volume fractions scale with aspect ratio $\phi_{\mathrm{I,N}} = m\xi^{1.36\pm0.07}$, where the prefactor $m$ strongly depends on size polydispersity for $\phi_{\mathrm{N}}$ but does not depend on size polydispersity for $\phi_{\mathrm{I}}$ with $\phi_{\mathrm{I}}$ and $\phi_{\mathrm{N}}$ being the volume fractions of the isotropic and the nematic phases on the cloud curves, respectively.

DOI: 10.1103/PhysRevE.85.061708 PACS number(s): 64.70.M−, 47.57.J−, 64.75.Xc, 82.70.Kj

## I. INTRODUCTION

Many materials and biological systems in nature are mainly suspensions composed of disks, such as clay [1–3], asphaltenes [4,5], histone octamer disks in nucleosomes [6], and red blood cells [7]. Theoretical studies [8,9] and computer simulations [10–12] have confirmed that disks can undergo different liquid crystal transitions at high concentrations due to their excluded volumes. The discotic liquid crystalline phases can acquire exceptional thermal, electrical, and mechanical properties [13,14]. Liquid crystals [8,9,15,16] with distinctive flow behaviors are of great fundamental and technological importance. Regardless of their natural abundance, studies of disks are less commonly undertaken than studies of rods [17,18]. However, two-dimensional disks behave quite differently compared to one-dimensional rods as manifested by the following observation in the limit case: Infinitesimally thin disks in thickness have a nonzero excluded volume proportional to $0.5\pi D^3\langle\sin\gamma\rangle$, where $D$ is the disk diameter, $\gamma$ is the angle between two disks' orientations, and $\langle\rangle$ stands for the thermodynamic average [9]; whereas, rods of vanishing diameter have a zero excluded volume proportional to $2l_r^2 D_r\langle\sin\gamma\rangle$, where $l_r$ is the length of the rods and $D_r$ is the diameter [19]. For liquid crystals, the discotic nematic phase has long been elusive of observation [20]; whereas, nematic phases are frequently observed for calamitic (rod) liquid crystals.

The discotic isotropic-nematic (I-N) transition will play an important role in understanding the fundamentals of soft condensed matter in science and technology [21]. The study of this transition can facilitate an understanding of the behavior of asphaltenes [5] to produce soft matrices of functional molecules [22], to promote the disklike mesogens to be used as templates for the preparation of mesoporous materials [23,24], and to initiate the use of nanoplatelets in semiconductors [21] and solid state photovoltaic cells [25]. In addition, a better understanding of the optical and electronic properties [26,27] of the nematic discotic phase can serve in the development of new liquid crystal display (LCD) devices [24,28,29]. The importance to LCDs relies on the fact that the discotic nematic phase is characterized by low viscosity and can easily be reoriented by applying electric fields, magnetic fields, and shear stimuli.

A representative phase diagram of colloidal disks contains phases, such as isotropic (I), nematic (N), columnar (C), smectic (S), and crystalline (X). The diagrams depend substantially on the disk aspect ratio ($\xi = L/D$ = thickness/diameter) [12] and polydispersity in terms of particle diameter ($\sigma$) [30]. Generally speaking, polydispersity greatly alters the phase diagram. It is well known that crystallization of hard spheres can be suppressed by the presence of a moderate polydispersity ($\sigma \sim 10\%$) [31]. There are I-N and N-C transitions for relatively low polydispersed discotic suspensions ($\sigma < 17\%$) [32,33] and an N-S transition for high polydispersities ($\sigma > 17\%$) [34–37].

Discotic suspensions have intrigued scientists since Langmuir in 1938 demonstrated that clay particles can exhibit a discotic nematic phase [38]. Around the 1940s, Onsager predicted the capability of platelets to make an I-N transition [8]. His theory was based on the excluded volume of disks with increasing translational entropy to compensate for the dismissing of orientational entropy [8,9]. The I-N transition has now become the most studied phase transition in science [15,37,39–42]. Computer simulations of the I-N transition have been carried out for cut spheres at aspect ratios smaller than [43,44] or larger than 0.1 [12,45,46], but due to the system size, it is not possible to confirm the first-order nature of the I-N transition. By increasing system size, some simulations have revealed the possibility for a weak first-order I-N transition with an aspect ratio equal to 0.1 [12]. Interesting experimental results have also been published; for example, Lekkerkerker's group used sterically stabilized gibbsite particles [$Al(OH)_3$]

*zcheng@tamu.edu

 

at $\xi \sim 10$ in toluene [39] or electrostatically stabilized ones in water [47–50] to produce I-N transitions. van der Beek *et al*. [48] described how gravity developed a columnar phase at the bottom of an initial I-N biphasic sample elucidating the I-N-C triple point at $\xi \sim 0.143$. A study related to the competition among sedimentation, gelation, and liquid crystal formation of gibbsite suspensions was reported by Wijnhoven *et al*. [51]. Aqueous suspensions of $Ni(OH)_2$ at $\xi \sim 0.11$ were reported to present a columnar phase coexisting at equilibrium with an isotropic phase [52].

We are interested in studying the I-N transition at low aspect ratios ($\xi \ll 0.1$), which, thus far, has only been occasionally investigated. Inorganic layers obtained from exfoliation of lamellar crystals possess a highly anisotropic shape with a thickness of several nanometers and can exhibit liquid crystals [20,22,42]. A wide variety of mineral crystals have been exfoliated, such as layered double hydroxides [53], niobates [28,54–61], clay [38,62–64], phosphates [60,61,65–67], titanium oxides [60,68], and graphite [69]. I-N transitions have been achieved by using layers of Mg-Al double hydroxides (LDH) [70] and exfoliated niobate colloidal suspensions of $K_4Nb_6O_{17}$ [22]. The niobate crystal layers have a low aspect ratio, ranging from 0.0015 to 0.0035 so that birefringence occurs at low volume fractions. Dependence on the aspect ratio has been studied for the I-N transition of $K_4Nb_6O_{17}$ layers obtained by exfoliating pristine crystals using a well-defined sonication procedure [71]. It was found that the I-N transition occurred at higher volume fractions when the aspect ratio was increased. The polydispersity of the nanosheets, however, was not controlled, and the effect on the I-N was not carefully studied. Liquid crystalline behavior has also been reported for exfoliated $HNb_3O_8$ and $HTiNbO_5$ [72]. Clay presented a particular challenge for scientists due to gelation, even though laponite suspensions could exhibit an I-N phase transition [62], and these laponite suspensions presented clear-cut nematic textures and orientational ordering [63,64,73,74].

Here, we study the I-N transition using exfoliated $\alpha$-zirconium phosphate (ZrP) at different aspect ratios. The ability to control the lateral dimension of the ZrP crystals allows us to tune the aspect ratio of the nanoplates in a wide range. ZrP is a crystal configured by layers having the same thickness [75,76]. A layer of ZrP is composed of a $ZrO_6$ sheet coordinated with $HPO_4^{2-}$ tetrahedrons. The aspect ratio can be easily varied by fabricating ZrP crystals of different

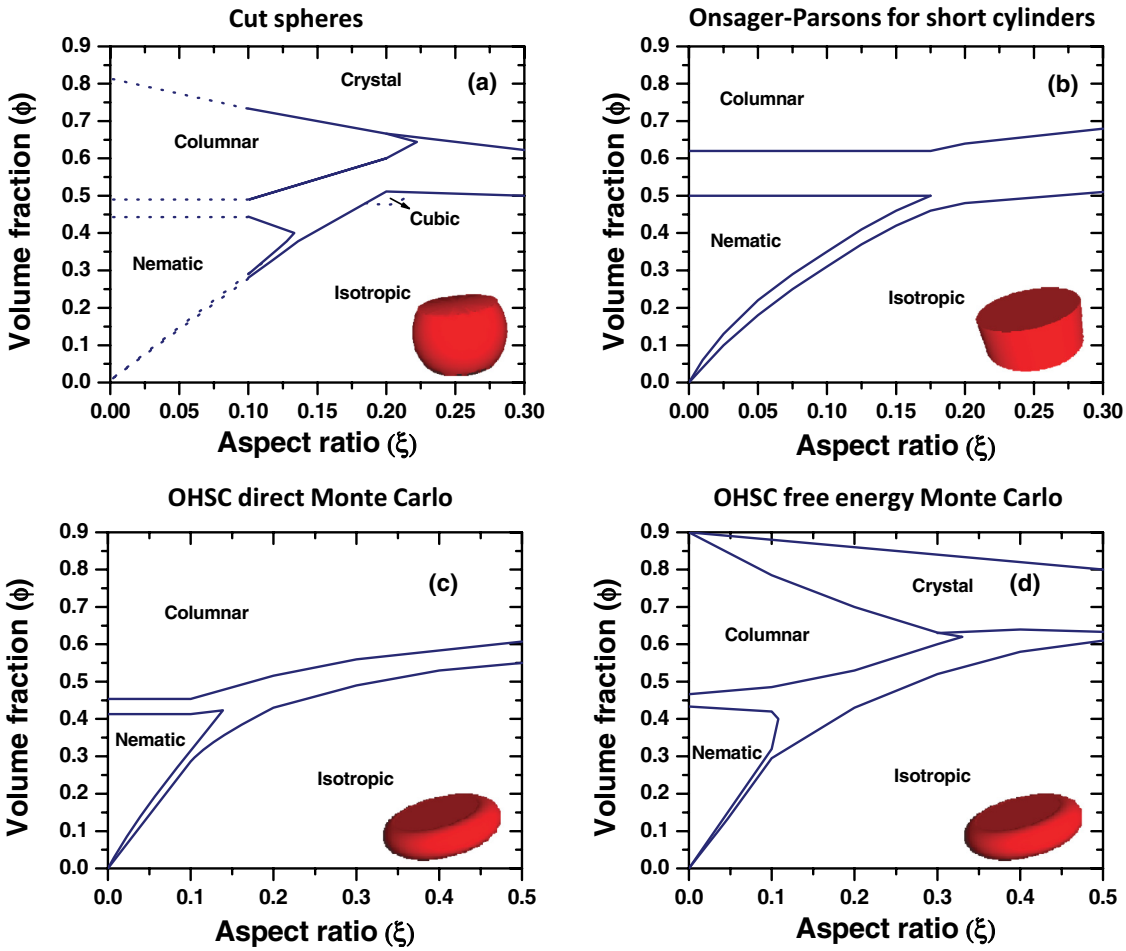


FIG. 1. (Color online) Phase diagrams for discotic systems in volume fraction ($\phi$) versus aspect ratio obtained from simulations. (a) A general diagram for cut spheres (*NVT*-MC). The dashed lines represent simulation data reported by Veerman and Frenkel for $\xi < 0.1$ [12], (b) short cylinders (Onsager-Parsons theory) [79], (c) oblate hard spherocylinders (*NPT*-MC) [80], and (d) oblate hard spherocylinders (free energy calculations) [81]. The insets at the bottom left of each graph illustrate the side view and the three-dimensional shape of the disks.

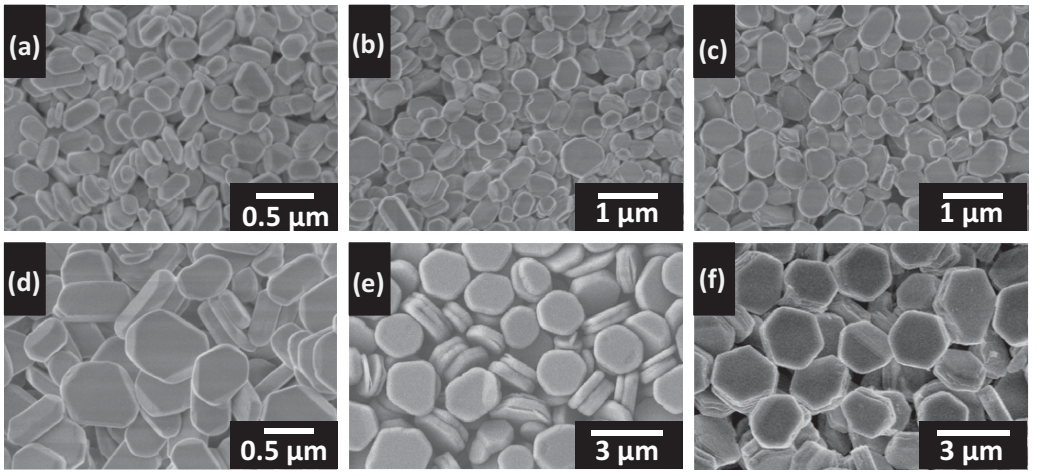


FIG. 2. Pristine $\alpha$-zirconium phosphate crystals. Scanning electron microscope micrographs of different ZrP sizes prepared at different conditions (a) 9$M$-5 h, (b) 12$M$-5 h, (c) 15$M$-5 h, (d) 9$M$-24 h, (e) 12$M$-24 h, and (f) 15$M$-24 h.

sizes followed by exfoliation through intercalation of guest molecules [i.e., tetrabutylammonium ($TBA^+$)] [77]. Using this technique, we are able to study the sedimentation for high and low aspect ratio platelets using ZrP [78]. Our work here examined the effects of aspect ratio and shape on I-N transition at the low aspect ratio region ($0.001 < \xi < 0.01$). The dependence of the positions of the biphasic gap for a fixed aspect ratio ZrP nanoplate on size polydispersity was elucidated. A power law scaling was found for the aspect ratio dependence of the phase transition volume fractions $\phi_{I,N}(\xi)$. Platelet size polydispersity was observed to separate the nematic volume fraction $\phi_N(\xi)$ further from the isotropic volume fraction $\phi_I(\xi)$, whereas, the position of $\phi_I(\xi)$ was not dramatically affected; hence, the effect of polydispersity would be more dramatic at higher aspect ratios (i.e., low degree of anisotropy).

## II. PREVIOUS RESULTS FROM SIMULATIONS

We compare here the aspect ratio-dependent phase diagrams in the literature for cut spheres using *NVT*-Gibbs ensemble (GE) [12], *NPT*-GE [46], and umbrella sampling (US) [43], which are different kinds of Monte Carlo (MC) simulations. We also examine the phase diagrams of hard platelike cylinders from Onsager-Parsons second virial theory [79] and of the oblate hard spherocylinders (OHSC) also known as discotic spherocylinders, which were obtained using direct energy calculations [80] and free energy calculations [81] via MC simulations.

### A. Cut spheres

Veerman and Frenkel ($\xi = 0.1$, 0.2, and 0.3, the number of particles $N = 256$ and 288 *NVT*-MC) [12], Piñeiro ($\xi = 0.1$, $N = 1500$ and 3000 *NPT*-GEMC) [46], and Fartaria and Sweatman ($\xi = 0.001$, 0.01, 0.04, 0.07, and 0.1, $N = 288$ and 2048 *NPT*-USMC) [43] studied the I-N phase transition in suspensions of hard cut spheres at various aspect ratios. A phase diagram for cut spheres is shown in Fig. 1(a). Piñeiro's results [46] were in agreement with Veerman and Frenkel's data [12]. For both simulations, the phase behavior of hard cut spheres was found to be strongly dependent on the aspect ratio. At $\xi = 0.1$, both nematic and columnar phases were reported; however, Piñeiro obtained larger I-N transition concentrations compared to Veerman and Frenkel [46]. This variation was attributed to the difference in system size or to a change in simulation technique (*NPT* versus *NVT* ensembles). Around $\xi = 0.2$, Veerman and Frenkel [12] found a columnar phase and a phase with cubic orientational order but no translational order, which was called the "cubic phase." The cubic phase is still under investigation to determine if

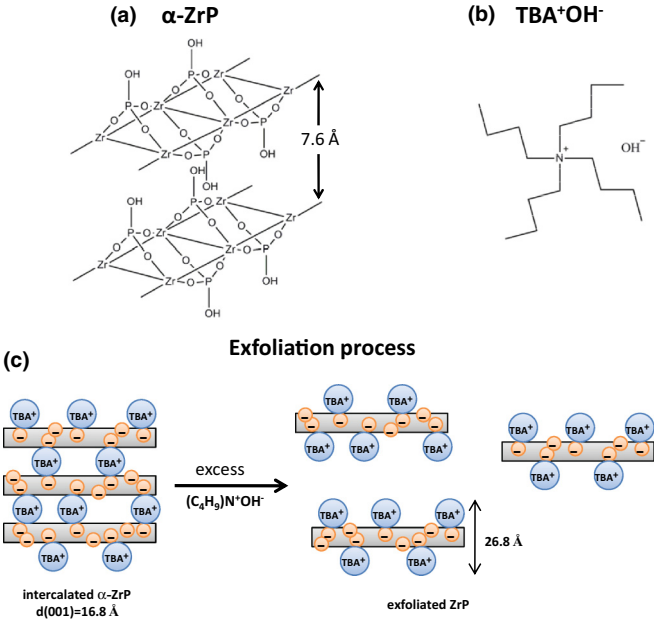


FIG. 3. (Color online) Structure of zirconium phosphate crystals and the exfoliation process. (a) Structure of crystalline ZrP. (b) Guest molecule: $n$-tetrabutylammonium hydroxide ($TBA^+OH^-$) and (c) schematic process of lamellar crystals going through exfoliation by using an excess of TBA. After exfoliation, monolayers were obtained having a thickness of 26.8 Å.

the stability is only temporary [81–84]. For $\xi = 0.3$, only isotropic and crystal phases were obtained. For cut spheres at low aspect ratios, Fartaria and Sweatman [43] found that the nematic-order parameter $S_2$ depended strongly on aspect ratio $\xi$. $S_2 = 1/2(\cos\theta^2 - 1)$ is a measure of the average relative orientation of the disks that is close to 0 in the isotropic phase and nonzero in the nematic phase [85], where $\theta$ is the average inclination of the platelets to the director. The nematic-order parameter presents a value close to 1 for the nematic phase at $\xi = 0.1$ and approximately 0.5 for the smaller aspect ratios ($\xi = 0.001$, 0.01, and 0.04). Fartaria and Sweatman [43] found that, in simulations, a constant I-N transition gap occurred for low aspect ratios ($\xi \leqslant 0.04$). At $\xi \geqslant 0.1$, the possibility for formation of the nematic phase was reduced, and the formation of the columnar phase was preferred [43].

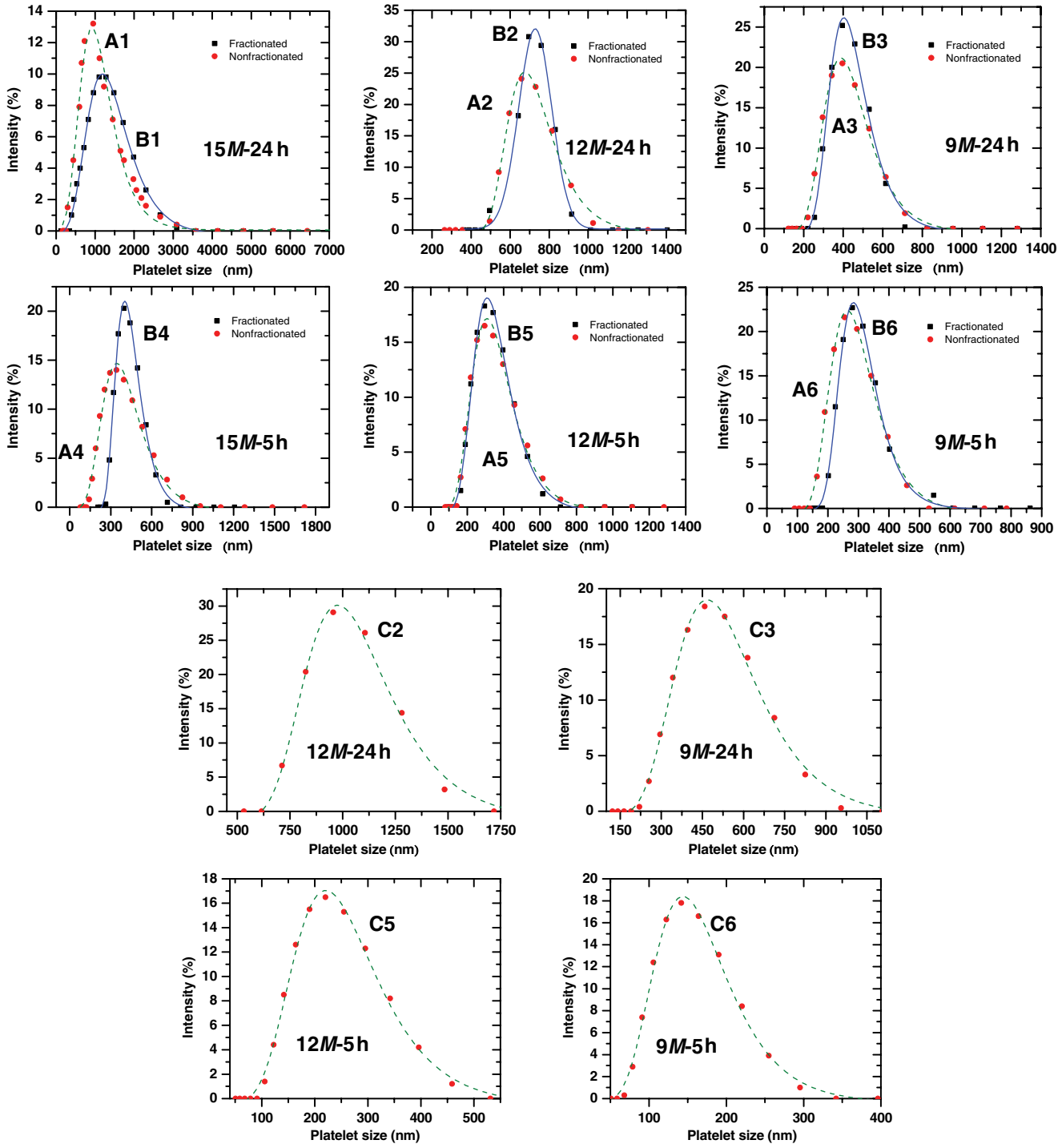


FIG. 4. (Color online) Size distribution for exfoliated ZrP platelets as measured by DLS. Aspect ratio and polydispersity obtained are listed in Table I. The nonfractionated and the fractionated samples are represented by the green-dashed (gray dashed) red circles and the blue-lined (black-lined) black squares, respectively. The lines are fit to the extreme distribution function.

TABLE I. Characterization of the exfoliated ZrP platelets.

| | Nanoplate size (nm) | | | Polydispersity ($\sigma$) | | | Aspect ratio ($\xi$) | | |
|---|---|---|---|---|---|---|---|---|---|
| Sample | A | B | C | A | B | C | A | B | C |
| ZrP(9*M*-5 h) (6) | 331 ± 87 | 367 ± 107 | 214 ± 62 | 25 ± 1% | 24 ± 1% | 29 ± 2% | 0.0081 ± 0.0020 | 0.0073 ± 0.0020 | 0.013 ± 0.004 |
| ZrP(12*M*-5 h) (5) | 400 ± 146 | 536 ± 162 | 377 ± 121 | 31 ± 2% | 28 ± 1% | 32 ± 2% | 0.0067 ± 0.0030 | 0.0050 ± 0.0020 | 0.0071 ± 0.0020 |
| ZrP(15*M*-5 h) (4) | 653 ± 206 | 687 ± 132 | | 35 ± 2% | 26 ± 1% | | 0.0041 ± 0.0010 | 0.0039 ± 0.0010 | |
| ZrP(9*M*-24 h) (3) | 957 ± 147 | 992 ± 173 | 776 ± 225 | 27 ± 2% | 22 ± 2% | 29 ± 2% | 0.0028 ± 0.0005 | 0.0027 ± 0.0005 | 0.0035 ± 0.0010 |
| ZrP(12*M*-24 h) (2) | 1276 ± 303 | 1410 ± 369 | 1604 ± 320 | 23 ± 1% | 18 ± 1% | 20 ± 1% | 0.0021 ± 0.0005 | 0.0019 ±0.0005 | 0.0017 ± 0.0004 |
| ZrP(15*M*-24 h) (1) | 2233 ± 807 | 2436 ± 562 | | 39 ± 2% | 28 ± 1% | | 0.0012 ± 0.0005 | 0.0011 ± 0.0003 | |

### B. Onsager-Parsons approximation for flat cylinders

Wensink and Lekkerkerker [79] studied the hard colloidal platelet phase diagram for different aspect ratios using Onsager's second virial theory with the Parson-Lee decoupling approximation for multiple body interactions. The phase diagram shown in Fig. 1(b) is compatible with other simulations [12,43,46,80,81]. As $\xi \sim 0$, the I-N concentrations are the same as those predicted by Onsager's second virial theory [86]. When the aspect ratio varies, the I-N transition concentrations increase with $\xi$, but the N-C density stays constant. The nematic order appears when the excluded volume exceeds a value of about 4, whereas, the columnar order becomes stable at a volume fraction ($\phi$) of around 0.4. The calculated triple point (I-N-C) position, which occurs at $\xi = 0.175$, deviates

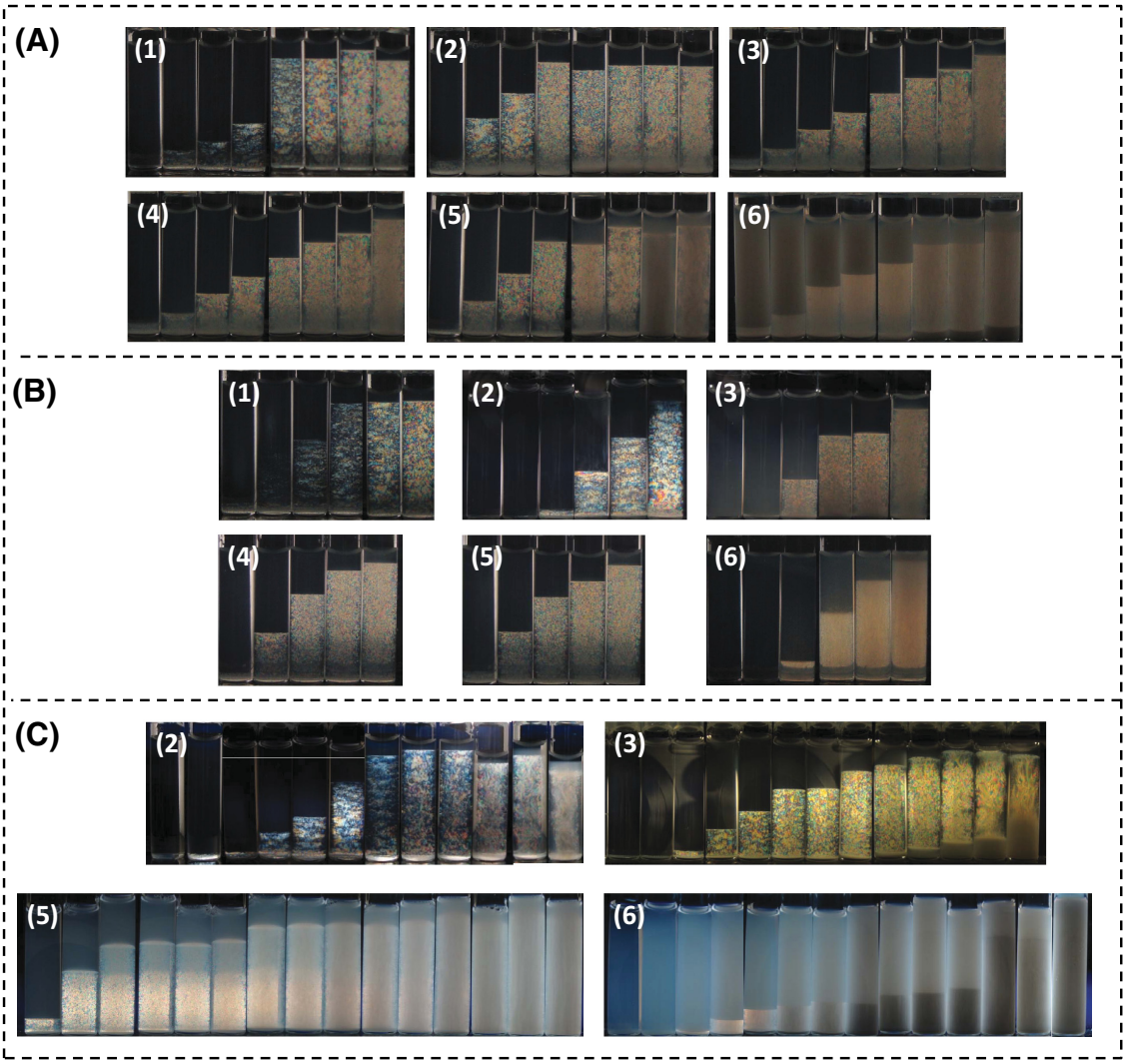


FIG. 5. (Color online) Suspensions of ZrP monolayers at various aspect ratios and different concentrations. (A1)–(A6) are the nonfractionated suspensions, and (B1)–(B6) are the fractionated suspensions. (C2)–(C6) are additional ZrP suspensions. Photographs were taken for samples set between cross polarizers to distinguish between upper isotropic and lower birefringent nematic liquid crystalline phase.

considerably from the aspect ratio values predicted by the other simulations, which occur at $\xi \sim 0.126$ [87,88] and $\xi \sim 0.14$ [12,44]. This deviation was caused mainly by the theoretical concentration value of the N-C transition exceeding that of the other simulations, resulting in a much higher intersection point. When $\xi > \xi_{\text{I-N-C}}$, the disks no longer exhibit an I-N transition, but rather an I-C transition. This theory, however, does not consider the cubic phase that was reported by Veerman and Frenkel [12]. In general, this approximation shows good agreement with the other simulations featured in Fig. 1 at $\xi > 0.1$.

### C. Oblate hard spherocylinders

The OHSCs have been extensively studied in recent years [80,81,89–91]. Figures 1(c) and 1(d) show the phase diagrams for OHSCs obtained using direct [80] and free energy calculations [81], respectively, using MC simulations. Both phase diagrams show similar tendencies when compared to the other simulations. The OHSCs' [80,81] [Figs. 1(c) and 1(d)] and the cut spheres' [Fig. 1(a)] [12,43,46] phase diagrams are similar based on the presence of their circular face shape [92]. In general, the isotropic phase is present for all aspect ratios, whereas, the nematic phase appears only at low aspect ratios ($\xi \leqslant 0.1$). The first-order I-N transition at $\xi = 0.1$ evident for the MC OHSC simulations [Figs. 1(c) and 1(d)] is comparable to that of the cut spheres [46] [Fig. 1(a)]. In the cut spheres simulation, an I-N biphasic gap was not obtained due to the inadequate number of particles used. Marechal *et al*. [81] stated that the packing fractions between cut spheres and OHSCs at low aspect ratios differed. By increasing the disk concentration at a range of $0 \leqslant \xi \leqslant 0.3$, the OHSCs can form either straight or tilted columns due to their shape. In

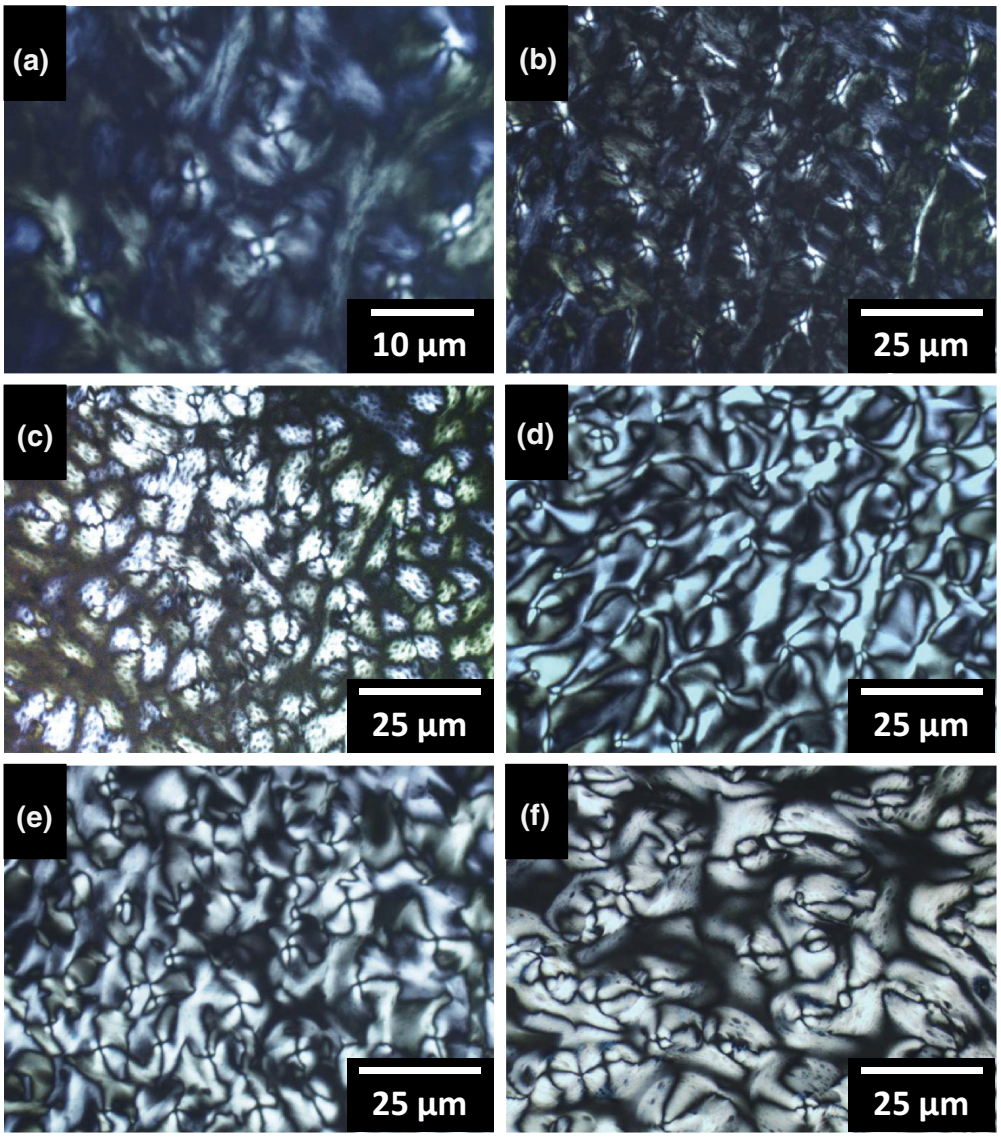


FIG. 6. (Color online) Cross-polarized optical microscopic images of nematic Schlieren textures at different aspect ratios. Aspect ratio increases from (a) to (f), which are from samples of B1 to B6, and (a) $\phi = 0.0053$, (b) $\phi = 0.01$, (c) $\phi = 0.014$, (d) $\phi = 0.02$, (e) $\phi = 0.0420$, and (f) $\phi = 0.06$. The micrographs were taken using a Nikon microscope TE-2000U with crossed polarizers. Picture of (a) was taken using 10× magnification, and pictures of (b)–(f) were taken using 4× magnification.

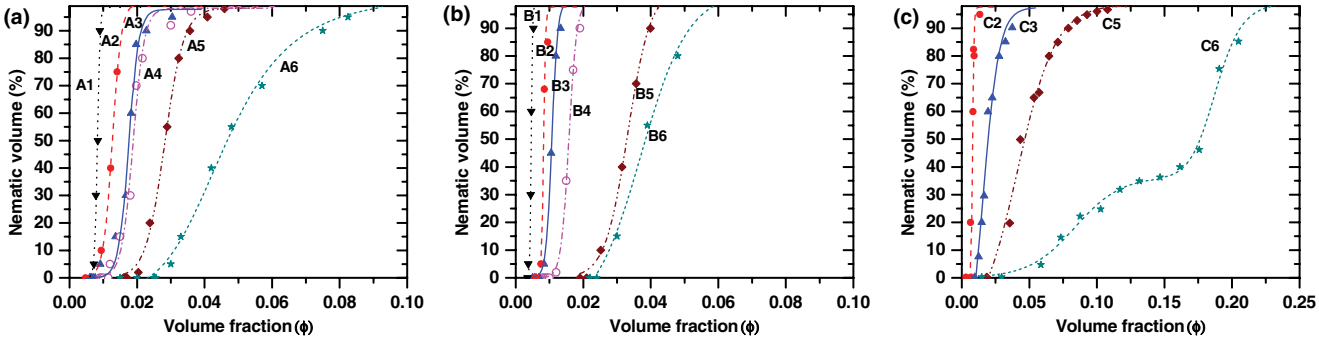


FIG. 7. (Color online) The relative fraction percentage of the nematic phase as a function of the monolayer volume fraction $\phi$. (a) The nonfractionated suspensions, (b) the fractionated suspensions, and (c) the additional ZrP suspensions. Aspect ratio increases from A1 to A6, from B1 to B6, and from C2 to C6. The values for aspect ratio and polydispersity can be found in Table I.

the N-C transition ($0 \leqslant \xi \leqslant 0.1$), the self-assembly of the disks at a very low aspect ratio ($\xi \ll 0.1$) does not favor disk interactions on the edge since the edge has a lower surface area than the faces of the disks, which leads to the disks having a greater chance of maintaining a nematic order. But at higher aspect ratios in the N-C transition region, the edge surface area becomes comparable to that of the face surface area. Disks are able to pack laterally much more easily due to the greater surface area and have a greater tendency to transition from a nematic to a columnar order [91]. Also, a difference in the phase diagram of the OHSCs from the cut spheres' phase diagram is the absence of the cubic phase. At $\xi = 0.2$, a possible cubic phase was found for the OHSC phase diagram but ended up converting to the columnar phase [81].

## III. EXPERIMENTAL RESULTS WITH MONOLAYERS OF $\alpha$-ZrP

### A. Control of the size and aspect ratio of ZrP nanoplates

The pristine $\alpha$-ZrP crystals were synthesized by a hydrothermal method [93]. In a typical reaction, 6 g of $ZrOCl_2 \cdot 8H_2O$ were added to 60.0 ml of phosphoric acid ($H_3PO_4$) solution. The mixture was enclosed in an autoclave and was left in an oven at 200 °C. In Fig. 2, crystals with a lateral size of $331 \pm 87$, $400 \pm 146$, $653 \pm 206$, $957 \pm 147$, $1276 \pm 303$, and $2233 \pm 807$ nm were obtained from the following conditions ($H_3PO_4$ concentration-reaction time): 9$M$-5 h, 12$M$-5 h, 15$M$-5 h, 9$M$-24 h, 12$M$-24 h, and 15$M$-24 h, respectively. The crystals at different sizes possessed irregular hexagonal shapes as shown in [Figs. 2(a)–2(f)] (SEM-JEOL JSM-7500F).

To obtain monolayers of ZrP that were uniform in thickness, these layered crystals [Fig. 3(a)] were exfoliated by dispersing the crystals in de-ionized water and subsequently adding tetra-($n$-butyl ammonium) hydroxide ($TBA^+OH^-$, Sigma-Aldrich, 40% in water) at a molar ratio of 1:1 (ZrP:$TBA^+OH^-$) at 0 °C. The $TBA^+OH^-$ molecule is depicted in Fig. 3(b). The concentrated suspensions were treated under sonication for 1 h and were left for 3 days to ensure full intercalation of the TBA and complete exfoliation of the crystals [66]. A general exfoliation process is illustrated in Fig. 3(c). The size and varying polydispersities ($\sigma$) of the exfoliated platelets were calculated using a dynamic light scattering instrument [(DLS), ZetaPALS, Brookhaven Instruments Corporation, Holtsville, NY] to measure the translational and rotational diffusion of ZrP monolayers [78] since all the platelets have a fixed thickness of $2.68 \pm 0.02$ nm [66]. The size distributions are shown in Figs. 4(A1)–4(A6) as represented by the green-dashed (gray-dashed) red circles. The polydispersity values were obtained by an extreme distribution fit of the data and are listed in Table I.

### B. Control of size polydispersity of ZrP nanoplates via I-N fractionation

To analyze the effect of polydispersity at different aspect ratios, we performed I-N fractionation to control the polydispersity of our samples. For each aspect ratio, the concentrated ZrP monolayers' mother suspension was diluted to the I-N coexistence region where the nematic volume occupies approximately 50% of the total suspension after complete phase separation. Particle size segregation occurred

TABLE II. The biphasic gap ($\Delta\phi_{I-N} = \phi_N - \phi_I$) values for different aspect ratios and polydispersities.

| | $\phi_I$ | | | $\phi_N$ | | | $\Delta\phi_{I-N}$ | | |
|---|---|---|---|---|---|---|---|---|---|
| Sample | A | B | C | A | B | C | A | B | C |
| ZrP(9$M$-5 h)(6) | $0.023^{+0.003}_{-0.010}$ | $0.024^{+0.004}_{-0.008}$ | $0.062^{+0.010}_{-0.020}$ | $0.081^{+0.070}_{-0.012}$ | $0.055^{+0.045}_{-0.008}$ | $0.23^{+0.06}_{-0.03}$ | $0.058^{+0.070}_{-0.015}$ | $0.031^{+0.045}_{-0.011}$ | $0.17^{+0.06}_{-0.04}$ |
| ZrP(12$M$-5 h)(5) | $0.017^{+0.003}_{-0.005}$ | $0.020^{+0.003}_{-0.006}$ | $0.028^{+0.004}_{-0.010}$ | $0.044^{+0.035}_{-0.007}$ | $0.042^{+0.020}_{-0.006}$ | $0.13^{+0.05}_{-0.02}$ | $0.028^{+0.035}_{-0.008}$ | $0.022^{+0.020}_{-0.008}$ | $0.10^{+0.05}_{-0.02}$ |
| ZrP(15$M$-5 h)(4) | $0.0092^{+0.0014}_{-0.0030}$ | $0.010^{+0.002}_{-0.003}$ | | $0.038^{+0.030}_{-0.006}$ | $0.020^{+0.010}_{-0.003}$ | | $0.028^{+0.030}_{-0.006}$ | $0.01^{+0.010}_{-0.004}$ | |
| ZrP(9$M$-24 h)(3) | $0.0073^{+0.0010}_{-0.0030}$ | $0.0077^{+0.0012}_{-0.0020}$ | $0.012^{+0.002}_{-0.005}$ | $0.027^{+0.025}_{-0.004}$ | $0.014^{+0.007}_{-0.002}$ | $0.045^{+0.040}_{-0.007}$ | $0.020^{+0.025}_{-0.005}$ | $0.0066^{+0.0070}_{-0.0030}$ | $0.033^{+0.040}_{-0.008}$ |
| ZrP(12$M$-24 h)(2) | $0.0068^{+0.0010}_{-0.0020}$ | $0.0060^{+0.0009}_{-0.0010}$ | $0.0045^{+0.0007}_{-0.0010}$ | $0.018^{+0.010}_{-0.003}$ | $0.010^{+0.002}_{-0.002}$ | $0.010^{+0.005}_{-0.002}$ | $0.011^{+0.010}_{-0.003}$ | $0.0044^{+0.0020}_{-0.0020}$ | $0.0055^{+0.0050}_{-0.0020}$ |
| ZrP(15$M$-24 h)(1) | $0.0041^{+0.0006}_{-0.0010}$ | $0.0033^{+0.0005}_{-0.0010}$ | | $0.010^{+0.007}_{-0.002}$ | $0.0052^{+0.0030}_{-0.0008}$ | | $0.0059^{+0.0070}_{-0.0020}$ | $0.0019^{+0.0030}_{-0.0010}$ | |

TABLE III. Isotropic ($\phi_I$) and nematic ($\phi_N$) volume fractions for aspect ratios ($\xi$) of 0.010 ± 0.003 and 0.0020 ± 0.0005 at different polydispersities ($\sigma$). The concentrations at zero polydispersity for both graphs were obtained from simulations of Fartaria and Sweatman [43].

| Aspect ratio ($\xi$) | Polydispersity ($\sigma$) | Isotropic ($\phi_I$) | Nematic ($\phi_N$) |
|---|---|---|---|
| 0.010 ± 0.003 | 0% | 0.026 | 0.027 |
| | 24 ± 1% | $0.024^{+0.004}_{-0.008}$ | $0.055^{+0.045}_{-0.008}$ |
| | 25 ± 1% | $0.023^{+0.003}_{-0.010}$ | $0.081^{+0.070}_{-0.012}$ |
| | 29 ± 2% | $0.062^{+0.010}_{-0.020}$ | $0.23^{+0.06}_{-0.03}$ |
| 0.0020 ± 0.0005 | 0% | 0.0052 | 0.0056 |
| | 18 ± 1% | $0.0060^{+0.0009}_{-0.0010}$ | $0.010^{+0.002}_{-0.002}$ |
| | 20 ± 1% | $0.0045^{+0.0007}_{-0.0010}$ | $0.010^{+0.005}_{-0.002}$ |
| | 23 ± 1% | $0.0068^{+0.0010}_{-0.0020}$ | $0.018^{+0.010}_{-0.003}$ |

as described in previous simulations [16] with larger-sized monolayers populating the nematic phase, reducing the size polydispersity of both the lower (N) and the upper (I) phases. This nematic phase was collected and the size distribution, labeled B1–B6 in Fig. 4, was compared to the original suspension A1–A6 in Fig. 4. The results show a slight increase in platelet size and a significant reduction of polydispersity (more than 5%) for highly polydispersed samples ($\sigma > 25\%$). Furthermore, we fabricated more ZrP suspensions using ZrP crystals synthesized from the following conditions: 12$M$-24 h, 9$M$-24 h, 12$M$-5 h, and 9$M$-5 h to expand the experimental set of samples, but the I-N crystal fractionation was not performed. The size distributions of these additional samples are labeled as C2, C3, C5, and C6 in Fig. 4 for notation and comparison purposes.

For each aspect ratio of varying polydispersities, samples of decreasing concentrations were prepared by diluting a concentrated suspension into 8-mm × 40-mm borosilicate glass cylinders (Fisher Scientific, Pittsburgh, PA). The suspensions were left at room temperature for 5 days until equilibrium was reached, and the phases were separated by sedimentation with a clear interface. The I-N phase behavior was analyzed by placing the tubes between two crossed polarizers and was photographed using a Sony DSC-W220 digital camera (Fig. 5).

Polarized photographs of completely phase-separated suspensions are shown in Fig. 5. As the concentration of exfoliated layers of ZrP increases, a birefringent nematic phase starts to appear at the bottom of the samples. We confirmed the presence of the characteristic nematic Schlieren textures using an optical microscope (TE-2000U, Nikon) for each aspect ratio [Figs. 6(a)–6(f)]. The texture observed between cross polarizers displays dark brushes having irregular curved shapes corresponding to extinction positions of the nematic liquid. Disclinations of $s = \pm 1/2$ and $s = \pm 1$, characteristics of nematic textures, were observable [94]. The nematic fraction increased as the platelet concentration increased in the coexistence region until full nematic phase was reached (Fig. 5). We measured the height of the nematic portion in the samples in Fig. 5 to determine the percentage of the nematic phase of each sample (Fig. 7).

It was possible to determine $\phi_I$ and $\phi_N$ from data extrapolation fitting with a logistic function $H = a/\{1 + \exp[-k(\phi - \phi_c)]\}$, where $H$ is the relative fraction percentage of the nematic phase, $a$ is the upper asymptote, $k$ is the increase rate of the nematic height with respect to the increase in sample volume fraction, and $\phi_c$ is the concentration at the maximum rate. $\phi_I$ (set $H_I/a = 0.025$) and $\phi_N$ (set $H_N/a = 0.98$) are the volume fractions on the boundaries of the I-N phase transition. The errors for $\phi_I$,$\phi_N$ are $(\delta a + \delta H_{I,N})/(a - H_{I,N}) + \delta H_{I,N}/H_{I,N} +$

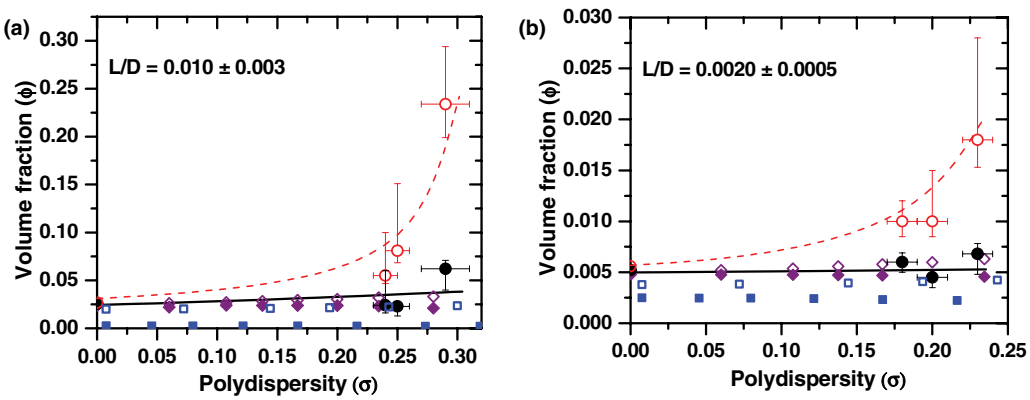


FIG. 8. (Color online) Volume fraction ($\phi$) of the solid black circles: isotropic and open red-gray circles: nematic volume fraction of the cloud phases as a function of polydispersity ($\sigma$) at fixed aspect ratios of around (a) 0.010 and (b) 0.0020. The concentrations at zero polydispersity for both graphs were obtained from simulations of Fartaria and Sweatman [43]. The lines are guides for the eye. The solid and open blue-black squares are the theoretical $\phi_I$ and $\phi_N$, respectively, from Sun *et al.* using a DFT calculation with Zwanzig approximation [37]. The solid and the open purple-black diamonds are the theoretical $\phi_I$ and $\phi_N$, respectively, from Bates and Frenkel for infinitely thin plates [16].

TABLE IV. Classification of ZrP suspensions according to polydispersity.

| Polydispersity group | A | B | C |
|---|---|---|---|
| i (33 ± 3%) | 1, 4, 5 | N/A | 3, 5, 6 |
| ii (27 ± 2%) | 2, 3, 6 | 1, 4, 5 | N/A |
| iii (21 ± 3%) | N/A | 2, 3, 6 | 2 |

$\delta\phi_c + \delta\phi_{sample}$, where $\delta\phi_{sample}$ is the error introduced via sample preparation. The error contribution from $k$ was ignored. The biphasic gap was then calculated as $\Delta\phi_{I-N} = \phi_N - \phi_I$. The measured biphasic values ($\Delta\phi_{I\text{-}N}$) are listed in Table II.

### C. The effect of polydispersity on the I-N transition at a fixed aspect ratio

The effect of disk size polydispersity on the I-N transition was studied and was compared to computer simulation results. Two aspect ratio groups of $0.010 \pm 0.003$ and $0.0020 \pm 0.0005$ of ZrP samples were used. From Table I, we selected A6, B6, and C6 for group 1; and A2, B2, and C2 for group 2. For $\sigma = 0$, we used the results obtained by Fartaria and Sweatman [43]. The isotropic ($\phi_I$) and nematic ($\phi_N$) volume fractions at aspect ratios of 0.010 and 0.0020 were calculated to be $\phi_I = 0.026$ and $\phi_N = 0.027$ and $\phi_I = 0.0052$ and $\phi_N = 0.0056$, respectively, using $\phi = (9/8)(\xi)(\rho D^3)(1/3)^{1/2}$ [48]. Table III contains the volume fraction concentrations ($\phi_I$,$\phi_N$) and the polydispersity ($\sigma$) values. We plotted $\phi_I$ and $\phi_N$ as a function of polydispersity for $0.010 \pm 0.003$ and $0.0020 \pm 0.0005$ groups in Figs. 8(a) and 8(b), respectively. It was observed that polydispersity had a great influence on the position of the I-N transition. As the polydispersity of suspensions increases, the biphasic gap broadens. In a recent paper [37] and in Bates and Frenkel [16], it was shown, from density functional theory (DFT) calculation and computer simulations, that an increase in polydispersity slightly decreases $\phi_I$ but increases $\phi_N$; therefore, the I-N transition widens with polydispersity in agreement with our observation here. The DFT calculation there also showed a large biphasic gap at $\sigma = 0$ in contrast with the narrow gap reported by Bates and Frenkel [16] at an aspect ratio around zero. Figure 8 also shows that DFT theory predicted a slower variation with size polydispersity compared to our experimental results. Fartaria and Sweatman [43] studied the dependence of the biphasic gap in the low aspect ratio region. In comparison, the simulation is consistent with our experimental ZrP results for $\phi_I$, however, differs for $\phi_N$ due to polydispersity in our experiments (Table III). Therefore, we can conclude that polydispersity does not affect $\phi_I$ values but has a large effect on the $\phi_N$ values. In simulations, the I-N transition is weakly first order when polydispersity is zero [33]. But in our experiments, fractionation occurs due to polydispersity where the large platelets populate the nematic phase and the smaller platelets stay in the isotropic phase. As a result, the biphasic gap becomes strongly first order [16,37].

### D. The effect of aspect ratio and polydispersity on the I-N transition

The combinational effect of aspect ratio and polydispersity on the I-N transition was evaluated. The isotropic transition volume fractions ($\phi_I$) of all ZrP samples were analyzed together since they were only slightly affected by polydispersity. In contrast, the nematic volume fractions ($\phi_N$) of the ZrP samples were studied in groups because they depended strongly on polydispersity. The samples were classified into groups i, ii, and iii for polydispersities of $33 \pm 3\%$, $27 \pm 2\%$, and $21 \pm 3\%$, respectively, as shown in Table IV. The transition boundaries are plotted in Fig. 9(a) where the solid black circles represent the isotropic phases and the red wine (dim gray) open triangles, orange (light gray) open circles, and red (dark gray) crosses represent the nematic phases for groups i, ii, and iii, respectively. Figure 9(a) shows that the biphasic gap ($\Delta\phi_{I-N}$) broadens as influenced by aspect ratio and polydispersity, implying that the nematic phase is favored at small aspect ratios and higher concentrations [8,18]. The values can be found in Table II. This behavior agrees with simulations from Bates and Frenkel [16] where disks having a low aspect ratio were found to have a higher nematic orientation compared to disks having a higher aspect ratio for a fixed concentration. In addition, Fartaria and Sweatman [43] affirmed that the

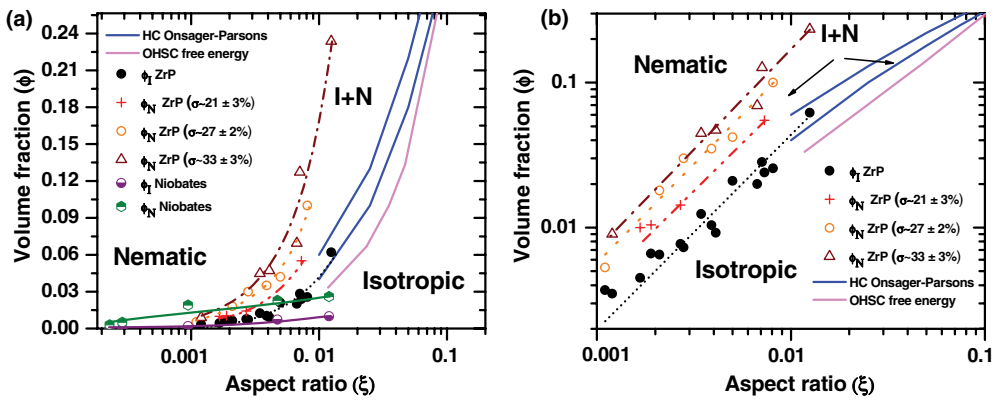


FIG. 9. (Color online) Comparison of the experimental $\phi_I$ and $\phi_N$ and simulation data. (a) Linear-logarithmic diagram illustrating the correspondence of the $\phi_I$ with the Onsager-Parsons theory and the OHSC free energy calculations. The difference in $\phi_N$ is due to effect of polydispersity of the ZrP platelets. The lines are guides for the eye. (b) Log-log diagram showing power law scaling of aspect ratio for $\phi_{I,\,i,\,ii,\,and\,iii} = 23.1 \pm 8.1\xi^{1.36\pm0.10}$ and $\phi_{N,i} = 115.5 \pm 78.6\,\xi^{1.41\pm0.20}$ $\phi_{N,ii} = 68.6 \pm 48.3\xi^{1.36\pm0.10}$ and $\phi_{N,iii} = 36.9 \pm 6.9\xi^{1.32\pm0.04}$ for groups i, ii, and iii, confirming that the width of the biphasic transition is affected by aspect ratio and polydispersity.

TABLE V. Comparison of experimental and simulations isotropic ($\phi_I$) and nematic ($\phi_N$) lines on power law $\xi$ scaling.

| Research | | Present paper (ZrP) | | | Onsager-Parsons theory [79] (short cylinders) | *NVT*-Monte Carlo [12] (cut spheres) |
|---|---|---|---|---|---|---|
| Polydispersity groups | | i ($\sigma_i \sim 33 \pm 3\%$) | ii ($\sigma_{ii} \sim 27 \pm 2\%$) | iii ($\sigma_{iii} \sim 21 \pm 3\%$) | $\sigma = 0$ | $\sigma = 0$ |
| $\phi_I$ | $m$ | | $23.1 \pm 8.1$ | | $1.87 \pm 0.10$ | $4.94 \pm 0.03$ |
| | $n$ | | $1.36 \pm 0.1$ | | $0.72 \pm 0.03$ | $1.20 \pm 0.04$ |
| $\phi_N$ | $m$ | $115.5 \pm 78.6$ | $68.6 \pm 48.3$ | $36.9 \pm 6.9$ | $2.11 \pm 0.20$ | Same as $\phi_I$ |
| | $n$ | $1.41 \pm 0.20$ | $1.36 \pm 0.10$ | $1.32 \pm 0.04$ | $0.83 \pm 0.03$ | |

first-order behavior of the I-N transition was more noticeable for larger aspect ratio ($\xi$) values. In Fig. 9(a), we also compare our study with the isotropic and nematic volume fractions obtained from niobate nanosheets represented as purple (dark gray) half-open circles and green (gray) half-open hexagons, respectively [71]. The niobates' isotropic line, except the data point around $L/D \approx 0.01$, is in agreement with ZrP. On the other hand, the nematic line does not overlap with the ZrP volume fractions.

Also, our experimental results are comparable with the Onsager-Parson theory for flat cylinders [79] and OHSC [80,81] illustrated as blue (black) lines and a light pink (light gray) line, respectively, in Figs. 9(a) and 9(b). The discrepancies of the ZrP from computer simulations might be due to a change in $\phi_I$ and $\phi_N$ by the particle shape and uniformity [92]. For instance, for different noncircular shapes (regular hexagons, pentagons, squares, triangles, ellipses, and rectangles), the width of the biphasic gap was found to be the same. However, the I-N transition decreases in volume fraction if the shape differs from the circular one [92].

In Fig. 9(b), a further analysis was obtained from a log-log plot of the experimental data in comparison to simulations and theory. The isotropic ($\phi_I$) and nematic ($\phi_N$) lines for the experiments and simulations [12,79] were fitted using a power law function $\phi = m\xi^n$ and were compared in Table V. In Fig. 9(b), it was observed that the I-N transition volume fractions for ZrP scales with the aspect ratio with a power law $\phi_{I,N} \sim \xi^{1.36\pm0.07}$. This result demonstrates that the broadening of the I-N transition strongly depends on polydispersity. As a result, the difference in the values of the parameters obtained from our experimental results from the simulations can be attributed to polydispersity [16], shape [92], and the interparticle interactions since simulations did not consider these factors. Assuming the shape of the platelets affects $\phi_I$ and $\phi_N$ in the same way [92], the biphasic gap ($\Delta\phi_{I-N}$) is essentially a function of polydispersity only. The position parameter ($m$) in the power law function depends on polydispersity and shape. Table V and Fig. 9 show that the exponent ($n$) slightly depends on polydispersity. Therefore, it becomes interesting to see why similar colloidal systems, such as clay, having a large size polydispersity and large aspect ratio ($\xi \sim 0.01$), commonly do not exhibit a nematic, but rather a gel phase, where some orientational order should be present [41,62,64,95]. In this paper, we observed that it was polydispersity that widened $\Delta\phi_{I-N}$. Large size polydispersity could be one of the factors preventing a fully nematic phase suspension for clay.

## IV. CONCLUSIONS

To summarize, our experiments revealed the effect of aspect ratio and polydispersity on the isotropic-nematic transition of colloidal suspensions of nanoplates that were uniform in thickness at the low thickness-to-diameter ratio limit. The aspect ratio of the nanoplates can be tailored by varying the size of ZrP crystals and a subsequent exfoliation with intercalation of tetrabutylammonium cations between the interlayers. The I-N transition widens as aspect ratio and polydispersity increase. The experimental data were compared to previous simulations, and the dissimilarities were attributed to size polydispersity and shape of the platelets. Extension of the present methodology can be applied to similar layered structures, such as montmorillonite [96], layered double hydroxides [53], and niobates [28,54–61,97]. The study of the I-N transition will allow further studies on liquid crystals' dependence on the aspect ratio, which will be a factor in tailoring optical, electrical, and mechanical properties of self-assembled discotic materials.

## ACKNOWLEDGMENTS

This work was supported by the NSF (Grant No. DMR-1006870) and the Mary Kay O'Connor Process Safety Center (MKOPSC) at Texas A&M University. We acknowledge useful discussions with Y. Martinez-Raton, E. Velasco, A. Clearfield, A. Diaz, H. J. Sue, D. Sun, and E. Risinger.

[1] J. J. Hao, K. V. Subbarao, and J. M. Duniway, Phytopathology **93**, 443 (2003).

[2] M. Moan, *Physical Chemistry of Colloids and Interfaces in Oil Production* (Institute Francais Du Petrole, Reuil, Paris, 1992).

[3] E. S. Boek, P. V. Coveney, H. N. W. Lekkerkerker, and P. van der Schoot, Phys. Rev. E **55**, 3124 (1997).

[4] S. Priyanto, G. A. Mansoori, and A. Suwono, Chem. Eng. Sci. **56**, 6933 (2001).

[5] M. D. Lobato *et al.*, Colloids Surf. A **298**, 72 (2007).
[6] J. Bednar *et al.*, Proc. Natl. Acad. Sci. USA **95**, 14173 (1998).
[7] M. Stefanini *et al.*, Blood **8**, 26 (1953).
[8] L. Onsager, Ann. N.Y. Acad. Sci. **51**, 627 (1949).
[9] P. A. Forsyth *et al.*, J. Chem. Soc., Faraday Trans. 2 **73**, 84 (1977).
[10] D. Frenkel and R. Eppenga, Phys. Rev. Lett. **49**, 1089 (1982).
[11] D. Frenkel and B. M. Mulder, Mol. Phys. **55**, 1171 (1985).
[12] J. A. C. Veerman and D. Frenkel, Phys. Rev. A **45**, 5632 (1992).
[13] E. Yasuda *et al.*, Mater. Sci. Eng. A **148**, 7 (2008).
[14] R. Verdejo *et al.*, J. Mater. Chem. **18**, 2221 (2008).
[15] F. M. van der Kooij, K. Kassapidou, and H. N. W. Lekkerkerker, Nature (London) **406**, 868 (2000).
[16] M. A. Bates and D. Frenkel, J. Chem. Phys. **110**, 6553 (1999).
[17] S. C. McGrother, D. C. Williamson, and G. Jackson, J. Chem. Phys. **104**, 6755 (1996).
[18] G. J. Vroege and H. N. W. Lekkerkerker, Rep. Prog. Phys. **55**, 1241 (1992).
[19] T. Odijk, Macromolecules **19**, 2313 (1986).
[20] J. C. P. Gabriel and P. Davidson, in *Colloid Chemistry 1* (Springer-Verlag, Berlin, 2003), p. 119.
[21] S. Ithurria *et al.*, Nature Mater. **10**, 936 (2011).
[22] N. Miyamoto and T. Nakato, Adv. Mater. **14**, 1267 (2002).
[23] F. Camerel, J. C. P. Gabriel, and P. Batail, Chem. Commun. (Cambridge) **2002**, 1926.
[24] F. Camerel, J. C. R. Gabriel, and P. Batail, Adv. Funct. Mater. **13**, 377 (2003).
[25] L. Kavan *et al.*, ACS Nano **5**, 9171 (2011).
[26] K. L. Woon *et al.*, Chem. Mater. **18**, 2311 (2006).
[27] M. Okazaki *et al.*, Polym. Adv. Technol. **11**, 398 (2000).
[28] F. E. Osterloh, J. Am. Chem. Soc. **124**, 6248 (2002).
[29] L. S. Li *et al.*, Nano Lett. **2**, 557 (2002).
[30] V. Germain and M. P. Pileni, Adv. Mater. **17**, 1424 (2005).
[31] D. A. Kofke and P. G. Bolhuis, Phys. Rev. E **59**, 618 (1999).
[32] J. A. C. Veerman and D. Frenkel, Phys. Rev. A **41**, 3237 (1990).
[33] M. A. Bates and D. Frenkel, J. Chem. Phys. **109**, 6193 (1998).
[34] H. H. Wensink and G. J. Vroege, J. Chem. Phys. **119**, 6868 (2003).
[35] A. Speranza and P. Sollich, J. Chem. Phys. **117**, 5421 (2002).
[36] N. Clarke *et al.*, J. Chem. Phys. **113**, 5817 (2000).
[37] D. Sun, H.-J. Sue, Z. Cheng, Y. Martínez-Ratón, and E. Velasco, Phys. Rev. E **80**, 041704 (2009).
[38] I. Langmuir, J. Chem. Phys. **6**, 873 (1938).
[39] F. M. van der Kooij and H. N. W. Lekkerkerker, J. Phys. Chem. B **102**, 7829 (1998).
[40] D. van der Beek, H. Reich, P. van der Schoot, M. Dijkstra, T. Schilling, R. Vink, M. Schmidt, R. van Roij, and H. Lekkerkerker, Phys. Rev. Lett. **97**, 087801 (2006).
[41] H. Hemmen *et al.*, Langmuir **25**, 12507 (2009).
[42] P. Davidson and J. C. P. Gabriel, Curr. Opin. Colloid Interface Sci. **9**, 377 (2005).
[43] R. P. S. Fartaria and M. B. Sweatman, Chem. Phys. Lett. **478**, 150 (2009).
[44] M. A. Bates and D. Frenkel, Phys. Rev. E **57**, 4824 (1998).
[45] A. Chamoux and A. Perera, J. Chem. Phys. **108**, 8172 (1998).
[46] M. M. Piñeiro, A. Galindo, and A. O. Parry, Soft Matter **3**, 768 (2007).
[47] D. van der Beek and H. N. W. Lekkerkerker, Europhys. Lett. **61**, 702 (2003).
[48] D. van der Beek and H. N. W. Lekkerkerker, Langmuir **20**, 8582 (2004).
[49] F. M. van der Kooij, D. van der Beek, and H. N. W. Lekkerkerker, J. Phys. Chem. B **105**, 1696 (2001).
[50] H. H. Wensink, G. J. Vroege, and H. N. W. Lekkerkerker, J. Phys. Chem. B **105**, 10610 (2001).
[51] J. Wijnhoven *et al.*, Langmuir **21**, 10422 (2005).
[52] A. B. D. Brown, S. M. Clarke, and A. R. Rennie, Langmuir **14**, 3129 (1998).
[53] M. Adachi-Pagano, C. Forano, and J. P. Besse, Chem. Commun. (Cambridge) **2000**, 91.
[54] M. M. J. Treacy *et al.*, Chem. Mater. **2**, 279 (1990).
[55] G. B. Saupe *et al.*, Chem. Mater. **12**, 1556 (2000).
[56] R. Abe *et al.*, Chem. Mater. **10**, 1647 (1998).
[57] R. Abe *et al.*, Chem. Mater. **9**, 2179 (1997).
[58] R. E. Schaak and T. E. Mallouk, Chem. Mater. **12**, 3427 (2000).
[59] N. Miyamoto *et al.*, Chem. Commun. **2002**, 2378.
[60] S. W. Keller, H. N. Kim, and T. E. Mallouk, J. Am. Chem. Soc. **116**, 8817 (1994).
[61] D. M. Kaschak *et al.*, J. Am. Chem. Soc. **121**, 3435 (1999).
[62] A. Mourchid *et al.*, Langmuir **11**, 1942 (1995).
[63] B. J. Lemaire *et al.*, Europhys. Lett. **59**, 55 (2002).
[64] J.-C. P. Gabriel, C. Sanchez, and P. Davidson, J. Phys. Chem. **100**, 11139 (1996).
[65] G. Alberti, M. Casciola, and U. Costantino, J. Colloid Interface Sci. **107**, 256 (1985).
[66] H.-N. Kim *et al.*, Chem. Mater. **9**, 1414 (1997).
[67] J. C. P. Gabriel *et al.*, Nature (London) **413**, 504 (2001).
[68] T. Sasaki *et al.*, J. Am. Chem. Soc. **118**, 8329 (1996).
[69] N. A. Kotov, I. Dekany, and J. H. Fendler, Adv. Mater. **8**, 637 (1996).
[70] S. Y. Liu *et al.*, Chem. Mater. **15**, 3240 (2003).
[71] N. Miyamoto and T. Nakato, J. Phys. Chem. B **108**, 6152 (2004).
[72] T. Nakato, N. Miyamoto, and A. Harada, Chem. Commun. (Cambridge) **2004**, 78.
[73] I. Bihannic *et al.*, Langmuir **17**, 4144 (2001).
[74] F. Cousin, V. Cabuil, and P. Levitz, Langmuir **18**, 1466 (2002).
[75] A. Clearfield and G. D. Smith, Inorg. Chem. **8**, 431 (1969).
[76] J. M. Troup and A. Clearfield, Inorg. Chem. **16**, 3311 (1977).
[77] A. A. Marti and J. L. Colon, Inorg. Chem. **42**, 2830 (2003).
[78] P. He, A. F. Mejia, Z. Cheng, D. Sun, H.-J. Sue, D. S. Dinair, and M. Marquez, Phys. Rev. E **81**, 026310 (2010).
[79] H. H. Wensink and H. N. W. Lekkerkerker, Mol. Phys. **107**, 2111 (2009).
[80] A. Cuetos and B. Martinez-Haya, J. Chem. Phys. **129**, 020701 (2008).
[81] M. Marechal *et al.*, J. Chem. Phys. **134**, 094501 (2011).
[82] P. D. Duncan, M. Dennison, A. J. Masters, and M. R. Wilson, Phys. Rev. E **79**, 031702 (2009).
[83] S. J. S. Qazi, G. Karlsson, and A. R. Rennie, J. Colloid Interface Sci. **348**, 80 (2010).
[84] R. Blaak, D. Frenkel, and B. M. Mulder, J. Chem. Phys. **110**, 11652 (1999).
[85] F. Gámez, P. J. Merkling, and S. Lago, Chem. Phys. Lett. **494**, 45 (2010).
[86] H. N. W. Lekkerkerker *et al.*, J. Chem. Phys. **80**, 3427 (1984).
[87] S. D. Zhang, P. A. Reynolds, and J. S. van Duijneveldt, J. Chem. Phys. **117**, 9947 (2002).
[88] D. van der Beek, T. Schilling, and H. N. W. Lekkerkerker, J. Chem. Phys. **121**, 5423 (2004).

[89] B. Martinez-Haya and A. Cuetos, J. Chem. Phys. **131**, 074901 (2009).
[90] B. Martinez-Haya and A. Cuetos, Mol. Simul. **35**, 1077 (2009).
[91] B. Martinez-Haya and A. Cuetos, Phys. Rev. E **81**, 020701 (2010).
[92] M. A. Bates, J. Chem. Phys. **111**, 1732 (1999).
[93] L. Y. Sun *et al*., New J. Chem. **31**, 39 (2007).
[94] P. G. Gennes, *The Physics of Liquid Crystals* (University Press, Oxford, 1974).
[95] N. I. Ringdal, D. M. Fonseca, E. L. Hansen, H. Hemmen, and J. O. Fossum, Phys. Rev. E **81**, 041702 (2010).
[96] D. R. Paul and L. M. Robeson, Polymer **49**, 3187 (2008).
[97] D. Yamaguchi, N. Miyamoto, T. Fujita, T. Nakato, S. Koizumi, N. Ohta, N. Yagi, and T. Hashimoto, Phys. Rev. E **85**, 011403 (2012).